



HAL
open science

A TEM study of exsolution in Ca-rich pyroxenes from the Paris and Renazzo chondrites: Determination of type I chondrule cooling rates

Priscille Cuvillier, Noel Chaumard, Hugues Leroux, Brigitte Zanda, Roger H. Hewins, Damien Jacob, Bertrand Devouard

► To cite this version:

Priscille Cuvillier, Noel Chaumard, Hugues Leroux, Brigitte Zanda, Roger H. Hewins, et al.. A TEM study of exsolution in Ca-rich pyroxenes from the Paris and Renazzo chondrites: Determination of type I chondrule cooling rates. *Meteoritics and Planetary Science*, 2018, 53 (3), pp.482-492. 10.1111/maps.13032 . hal-01765559

HAL Id: hal-01765559

<https://hal.science/hal-01765559v1>

Submitted on 11 Dec 2024

HAL is a multi-disciplinary open access archive for the deposit and dissemination of scientific research documents, whether they are published or not. The documents may come from teaching and research institutions in France or abroad, or from public or private research centers.

L'archive ouverte pluridisciplinaire **HAL**, est destinée au dépôt et à la diffusion de documents scientifiques de niveau recherche, publiés ou non, émanant des établissements d'enseignement et de recherche français ou étrangers, des laboratoires publics ou privés.



Distributed under a Creative Commons Attribution 4.0 International License

A TEM study of exsolution in Ca-rich pyroxenes from the Paris and Renazzo chondrites: Determination of type I chondrule cooling rates

Priscille CUVILLIER¹, Noël CHAUMARD^{2,3}, Hugues LEROUX ^{1,*}, Brigitte ZANDA^{2,4,5},
Roger H. HEWINS^{2,4}, Damien JACOB¹, and Bertrand DEVOUARD⁶

¹Unité Matériaux et Transformations, Université Lille 1 and CNRS, F-59655, Villeneuve d'Ascq, France

²Institut de Minéralogie, de Physique des Matériaux, et de Cosmochimie (IMPMC), Sorbonne Université, Muséum National d'Histoire Naturelle, UPMC Université Paris 06, IRD & CNRS, 75005 Paris, France

³WiscSIMS, Department of Geoscience, University of Wisconsin-Madison, 1215 W. Dayton Street, Madison, Wisconsin 53706-1692, USA

⁴Department of Earth and Planetary Sciences, Rutgers University, Piscataway, New Jersey 08854, USA

⁵Institut de Mécanique Céleste et de Calcul des Ephémérides, Observatoire de Paris, 77 Av. Denfert Rochereau, F-75014 Paris Cedex, France

⁶Aix-Marseille Université, CNRS, IRD, CEREGE UM34, 13545 Aix en Provence, France

*Corresponding author. E-mail: hugues.leroux@univ-lille1.fr

(Received 29 April 2016; revision accepted 13 November 2017)

Abstract—We conducted a transmission electron microscope study of the exsolution microstructures of Ca-rich pyroxenes in type I chondrules from the Paris CM and Renazzo CR carbonaceous chondrites in order to provide better constraints on the cooling history of type I chondrules. Our study shows a high variability of composition in the augite grains at a submicrometer scale, reflecting nonequilibrium crystallization. The microstructure is closely related to the local composition and is thus variable inside augite grains. For compositions inside the pyroxene miscibility gap, with a wollastonite (Wo) content typically below 40 mole%, the augite grains contain abundant exsolution lamellae on (001). For grain areas with composition close to Wo₄₀, a modulated texture on (100) and (001) is the dominant microstructure, while areas with compositions higher than Wo₄₀ do not show any exsolution microstructure development. To estimate the cooling rate, we used the spacing of the exsolution lamellae on (001), for which the growth is diffusion controlled and thus sensitive to the cooling rate. Despite the relatively homogeneous microstructures of augite grains with Wo < 35 mole%, our study of four chondrules suggests a range of cooling rates from ~10 to ~1000 °C h⁻¹, within the temperature interval 1200–1350 °C. These cooling rates are comparable to those of type II chondrules, i.e., 1–1000 °C h⁻¹. We conclude that the formation of type I and II chondrules in the proto-solar nebula was the result of a common mechanism.

INTRODUCTION

Chondrules are silicate spherules present in abundance in undifferentiated meteorites and they reveal extensive melting in the protoplanetary disk (e.g., Hewins et al. 1996; Zanda 2004). To date, the cause of the thermal events responsible for the melting is not fully constrained and the study of chondrule cooling rates can provide a better understanding of their formation mechanisms. Cooling rates of chondrules are

mainly estimated from the comparison of chondrule textures with those of synthetic chondrules obtained from crystallization experiments (e.g., Jones and Lofgren 1993; Lofgren 1996; Hewins et al. 2005). More quantitatively, cooling rates can be inferred from the study of FeO zonation in olivine embedded in type II chondrules (e.g., Jones 1990; Miyamoto et al. 2009). However, type II chondrules are mainly present in ordinary chondrites, leaving the thermal history of reduced (type I) chondrules, dominant in carbonaceous

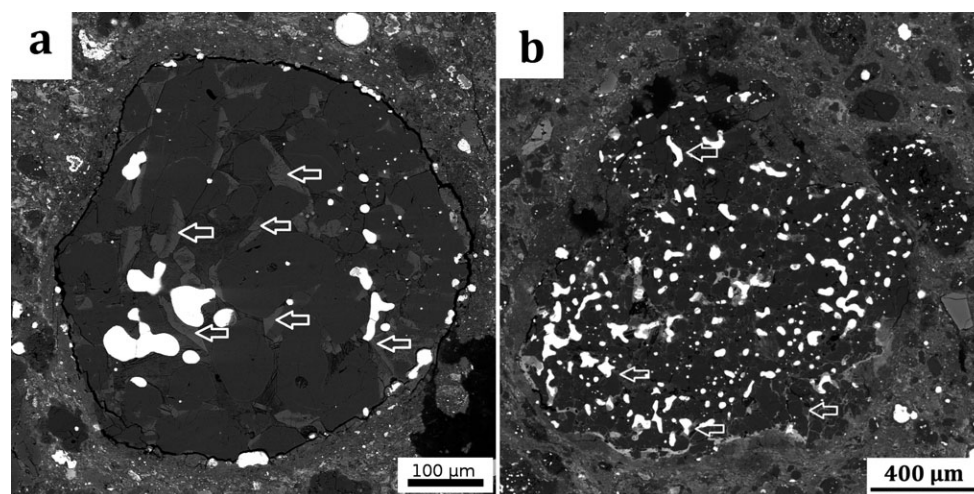


Fig. 1. SEM BSE image of the two IAB porphyritic chondrules from the Paris chondrite selected for the study. Enstatite and forsterite grains are dark gray and Ca-rich pyroxene light gray. Fe,Ni metal grains are white. Locations for which the FIB sections were extracted are indicated by white arrows. a) Chondrule P1. b) Chondrule P2.

chondrites, relatively poorly constrained (Radomsky and Hewins 1990; Wick and Jones [2012] and references therein). In order to decipher the thermal history of type I chondrules, other thermal indicators need to be found since forsterite grains are essentially unzoned. Recently, Cu-Ga diffusion profiles measured by LA-ICP-MS in metal grains were proposed to determine cooling rates of the host type I chondrules (Humayun 2012; Chaumard et al. 2014, 2015). Another method is based on the study of the exsolution microstructure in Ca-rich pyroxene present in type I chondrules (Weinbruch and Müller 1995).

Estimation of cooling rates from pyroxene exsolution was initiated by McCallister (1978) and applied to kimberlites. It was later used for other terrestrial or extraterrestrial samples (e.g., Grove 1982; Watanabe et al. 1985; Weinbruch and Müller 1995; McCallum and O'Brien 1996; Leroux et al. 2008). This method is based on the study of the coarsening of exsolution lamellae, which is a diffusion-controlled process and as such dependent on the cooling rate.

We have studied pyroxene exsolution lamellae in order to infer cooling rates of type I chondrules within the temperature interval of 1200–1350 °C, i.e., the formation interval of the exsolution lamellae, from the two carbonaceous chondrites Paris and Renazzo. The Paris CM meteorite contains both moderately and barely altered zones and is hence the least altered CM chondrite found so far (Hewins et al. 2014). Chondrules, which are mostly type I, represent about 45 vol% of the chondrite (Hewins et al. 2014). The Renazzo chondrite (CR2) experienced moderate aqueous alteration that mostly affected the matrix and the mesostasis of some chondrules (e.g., Weisberg et al.

1993). For Paris and Renazzo, type I chondrules are abundant and frequently contain Fe,Ni metal grains. In this study, we used analytical transmission electron microscopy (TEM) to study the pyroxene exsolution microstructure within two type I chondrules from the Paris meteorite and two from the Renazzo meteorite in order to assess their cooling rates.

SAMPLES AND METHODS

Scanning electron microscopy (SEM) was used to select suitable type I chondrules within the Paris and Renazzo meteorites. Backscattered electron (BSE) imaging and energy dispersive X-ray spectroscopy (EDS) compositional maps were obtained at 15 keV using a Tescan VEGA II LSU at IMPMC (MNHN-UPMC, Paris) in order to localize type IAB chondrules with porphyritic texture and containing Ca-rich pyroxene grains. Pyroxene grains are located interstitial to the forsterite phenocrysts. Typically, the Ca-pyroxene grains are euhedral with elongated shapes. They frequently contain a Ca-poor core (enstatite or pigeonite) showing that they overgrew on Ca-poor pyroxene. Two chondrules within each of the meteorites were selected for TEM observations, labeled P1 and P2 for Paris with a size of 0.5 and 1.5 mm in diameter, respectively, and labeled R1 and R2 for Renazzo with a size of 1 and 1.8 mm in diameter, respectively. Figure 1 shows the two selected chondrules in the Paris meteorite.

In the Paris meteorite, six TEM samples were extracted from P1 and four from P2, all taken from different Ca-rich pyroxene grains at different locations in the chondrule. This approach allowed us to check for the reproducibility of the exsolution microstructure in a

Table 1. Representative compositions of pyroxene grains extracted from the four studied chondrules. Data are given in atom% and are normalized to 100%. Absorption and k-factor correction have been applied. Uncertainties on the values are typically 3% for the major elements (Mg, Si, and Ca) and 10% on the minor elements (Al, Ti, Cr, Mn, and Fe).

Chondrule	O	Si	Mg	Ca	Al	Ti	Cr	Mn	Fe	Wo%
P1	60.1	18.9	13.1	4.95	2.40	0.04	0.24	nd	0.23	27
P1	60.2	18.9	15.4	1.26	2.71	0.03	0.43	0.28	0.68	7
P1	59.7	17.8	10.6	8.05	2.55	0.28	0.54	nd	0.47	42
P2	59.4	19.8	14.5	5.73	0.43	0.06	0.06	nd	0.04	28
P2	61.0	18.5	18.6	1.10	0.58	0.05	0.08	nd	0.06	6
P2	60.6	18.5	12.2	7.58	0.72	0.21	0.20	nd	0.01	38
R1	60.3	18.9	9.84	6.36	2.54	0.10	0.65	0.84	0.49	38
R1	59.7	18.1	12.4	5.46	1.56	0.10	0.72	0.79	1.18	29
R1	59.9	19.1	16.4	1.49	0.64	nd	0.54	0.81	1.11	8
R2	59.8	17.8	11.0	5.73	1.67	0.06	1.81	0.92	1.08	32
R2	59.7	18.5	13.1	5.53	1.39	nd	0.58	0.63	0.49	29
R2	59.7	18.4	11.4	7.21	1.27	nd	0.79	0.56	0.64	38

nd = not detected.

given chondrule. For Renazzo, one focused ion beam (FIB) sample per chondrule was studied in R1 and R2. TEM samples were prepared by the FIB technique using an FEI Strata DB 235 at IEMN (University of Lille). The size of the FIB sections was typically $15 \times 7 \mu\text{m}^2$ and 100 nm thick. The FIB sections should ideally be oriented as (010) sections of the pyroxene (space groups $C2/c$ and $P2_1/c$) in order to study both the exsolution lamellae oriented along the (001) plane and those that could develop along the (100) plane. To achieve this objective, the orientation of the FIB sections ($\sim 15 \mu\text{m}$ long dimension) was chosen along the elongation direction of the pyroxene grains, which is the favored growth direction and is usually along the c crystallographic axis.

Analytical TEM was performed using a FEI Tecnai G2-20 (LaB₆ filament) operating at 200 kV and a Philips CM30 (LaB₆ filament) operating at 300 kV (University of Lille). The study of the microstructure was performed using bright- and dark-field imaging in conventional TEM and annular bright- and dark-field detectors in scanning TEM. The crystallographic orientations of the grains were determined by selected area electron diffraction (SAED). The compositions of the pyroxene grains were measured using X-ray EDS. For the acquisition of the EDS data, we used the scanning TEM mode with a beam diameter within the range 5–15 nm. For quantitative chemical analyses by EDS, calculations of element concentrations and atomic ratios were performed using calibrated k-factors and thin film matrix correction procedure. The k-factors for the major elements (O, Al, Mg, Si, Ca, and Fe) were determined using standard specimens according to the

parameter-less method of Van Cappellen (1990). The absorption correction procedure based on the electroneutrality principle was applied (Van Cappellen and Doukhan 1994).

RESULTS

The FIB samples exhibit a high variability of microstructures, mainly due to a local variability in composition at the micrometer scale. First, we give a general description of the various microstructures observed in the different FIB sections. Then, we focus on the more detailed description of the microstructure (tweed textures and exsolutions).

General Overview of the FIB Sections

Table 1 gives representative compositions for the three pyroxene phases (enstatite, pigeonite, and augite) present in the FIB sections. Minor element concentrations are relatively high for Al, Ti, Cr, and Mn. In most samples, the FIB sections exhibit strong composition gradients, up to 10 Wo% on a few μm (Wo = Wollastonite component, given in mole% and considering only the Ca, Fe, and Mg content). For most samples (five in P1, three in P2, and the two R1 and R2 in Renazzo), the compositions are highly subcalcic relative to the CaMgSi₂O₆ endmember, and augite grains display varied microstructures. In two FIB samples (from P2 and R2), the augite grains are in contact with enstatite (Figs. 2 and 3). The enstatite contains planar defects along the (100) planes, which correspond to the alternation of clino-enstatite and ortho-enstatite lamellae on (100). Augite and enstatite

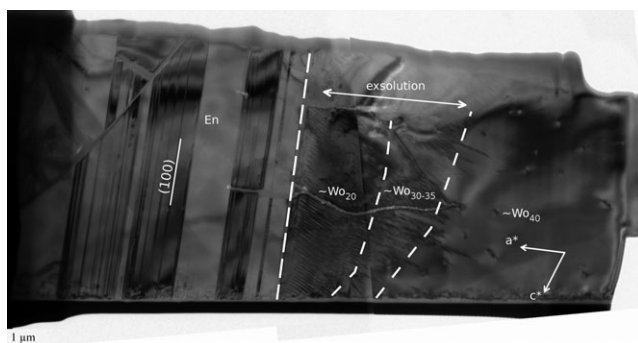


Fig. 2. Bright-field TEM image of a full FIB section extracted from a pyroxene grain in Paris chondrule P2. The left side of the grain consists of enstatite containing planar defects along the (100) plane. The right side of the grain is composed of Ca-rich pyroxene containing an exsolution microstructure on (001) (middle of the section). The Ca content of the grain increases from Wo_{20} to Wo_{40} from the left part (exsolved) of the augite grain to the right (un-exsolved).

are found in crystallographic relationships, with $(100)_{Au} // (100)_{En}$ suggesting an overgrowth process. In two other FIB samples (in P1 and R1), augite has an interface with pigeonite, both containing exsolution lamellae.

The composition profiles measured in the samples have a rather random shape with frequent abrupt local variations at distances less than a micrometer for some and constant composition for others. Figure 3 shows one of the composition profiles in R2 along which the averaged local Wo content varies from 35% to 27% over a distance of 3 μm .

Microstructure–Composition Relationships

The microstructure of the augite grains is strongly dependent on the composition. Two FIB sections (one in P1 and one in P2) do not exhibit any exsolution lamellae. In these two cases, the augite grains have compositions exceeding Wo_{40} . Most of the samples display a heterogeneous composition at a submicrometer scale (Figs. 2 and 3). For compositions locally higher than Wo_{40} , sample areas do not usually exhibit any substructure. For compositions between $\sim Wo_{45}$ and $\sim Wo_{35}$, the dominant microstructure consists of a modulated texture with small amplitude (named “tweed texture” in the following discussion) oriented along the (100) and (001) planes. For compositions between $\sim Wo_{40}$ and $\sim Wo_{20}$, exsolution lamellae along the (001) planes are present. This last range of composition basically corresponds to the two-phase domain of the pyroxene miscibility gap. It should be noted that there is a sharp compositional overlap between the three microstructural categories (no exsolution, tweed texture, and exsolution

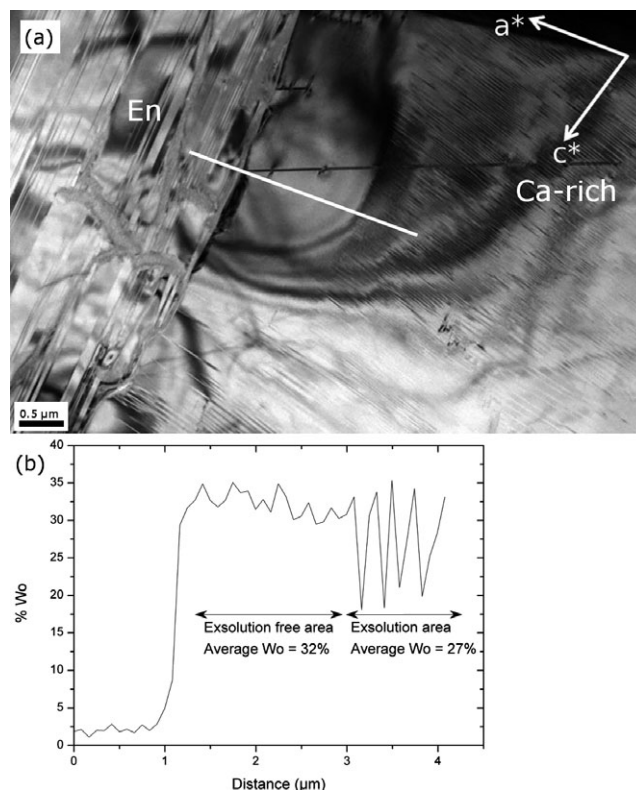


Fig. 3. a) Bright-field TEM image showing an interface between enstatite (left) and augite (right) in Paris chondrule P2. The enstatite grain contains planar defects on (100) and the augite grain contains exsolution lamellae on (001) except close to the interface with enstatite. b) Composition profile (Wo%) recorded by EDS across the interface enstatite/augite. The location of the profile is marked by a white line on the TEM image. The augite grain has a Wo content close to 35% at the interface decreasing to 27% over a distance of 3 μm in the augite grain. Note that exsolution is present for a concentration below Wo_{30} (right side of the profile). The presence of exsolution is the reason for the scattering of the Wo concentration in the exsolved region due to the presence of alternating Ca-poor (pigeonite) lamellae within the augite host and convolution of both under the electron beam.

along the (001) planes). Figure 4 summarizes the relationship between compositions and microstructures for the Paris chondrite, for which most of the data have been obtained.

In several samples, subgrain boundaries are present (Fig. 5a). They frequently separate areas with different composition, as illustrated by the composition profile of Fig. 5b taken across the subgrain boundary shown in Fig. 5a. In one sample (R2), we observed some tiny precipitates along the subgrain boundaries (Fig. 5c). Their small sizes (typically 20 nm) preclude the measurement of their individual compositions. EDS profiles taken across precipitates and the surrounding augite host display strong SiO_2 enrichments.

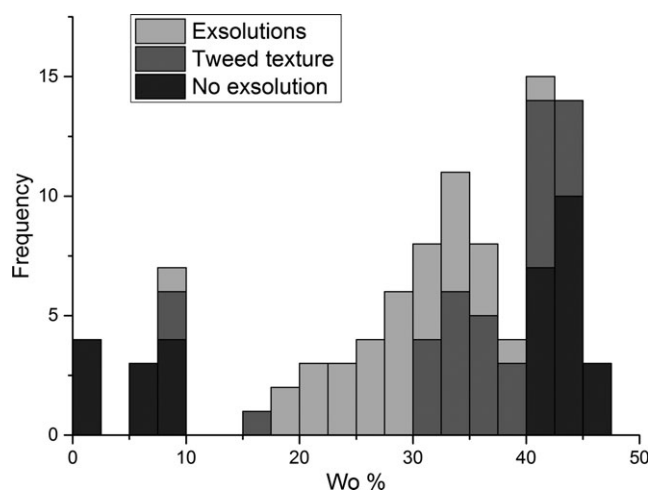


Fig. 4. Frequency diagram showing the composition (in $Wo\%$) of pyroxene from the two chondrules studied in the Paris meteorite, classified according to their microstructure. Typically, un-exsolved grains have Wo contents above Wo_{40} or below Wo_{10} , “tweed” grains have a Wo content between Wo_{30} and Wo_{45} , and exsolved grains have a Wo content between Wo_{08} and Wo_{40} .

Exsolution Microstructure and Tweed Texture

The average exsolution wavelength in each chondrule was deduced from the FIB sample areas using a statistical approach. The regions containing exsolution were divided into squares of $500 \times 500 \text{ nm}^2$. In each square, the average wavelength was measured and then reported in a diagram showing the distribution frequency as a function of the wavelength (Fig. 6). These statistical measurements were restricted to areas with compositions located inside the miscibility gap (from Wo_{11} to Wo_{33}) at $T = 1380 \text{ }^\circ\text{C}$. From the lamella periodicity distribution, we calculated a standard deviation value for each chondrule. The summary is shown in Table 2. The first column gives the range of the measured wavelengths in each chondrule. For P1 and P2, the wavelengths are within the range of 10–30 nm (average 19 nm) and 20–50 nm (average 30 nm), respectively (Figs. 7a and 7b). For R1 and R2, this range is 5–20 nm (average 14 nm) and 20–60 nm (average 35 nm), respectively (Figs. 7c and 7d).

Exsolution lamellae are lying along the (001) orientation. The lamellae are often slightly curved and display local interconnection. Selected area electron diffraction patterns taken on the pigeonite lamellae reveal the presence of $h+k$ odd reflections as well as a splitting of the diffraction spots along the a^* direction and oriented in the c^* direction (Fig. 8). The $h+k$ odd reflections are extinct in the augite $C2/c$ space group due to the C-centered lattice. The $h+k$ odd reflections

are characteristic of the low pigeonite $P2_1/c$ exsolved in the augite host $C2/c$. The splitting of the diffraction spots along the a^* direction is due to the difference in the β monoclinic angle between augite and pigeonite (about 3°).

For samples in which the exsolution lamellae are well developed (P2 and R2), the pigeonite lamellae contain antiphase boundaries (APBs), frequently parallel to (100) planes (Fig. 9). The domain size bordered by APBs is typically within the range of 10–20 nm. APBs separate two ordered domains of a crystal by a stacking fault in the translational symmetry. For the pigeonite, APBs are due to the displacive transformation of the high pigeonite $C2/c$ (disordered) to the low pigeonite $P2_1/c$ (ordered) with decreasing temperature (Morimoto and Tokonami 1969; Carpenter 1979; Buseck et al. 1980; Tribaudino 2000). The displacement vector between the two domains is $1/2(a+b)$, where a and b are the lattice parameters of the pigeonite (Morimoto and Tokonami 1969; Buseck et al. 1980).

Locally, some exsolution lamellae were observed along the (100) plane (Fig. 10). These lamellae are heterogeneously distributed and it was not possible to deduce an average spacing. It is likely that pre-existing defects, such as stacking faults, commonly observed in pyroxene grains, could have acted as a nucleating agent for the exsolution to occur. The samples having a composition between $\sim Wo_{35}$ and $\sim Wo_{45}$ or a composition close to Wo_{10} frequently show a tweed texture with (100) and (001) orientations (Fig. 11).

DISCUSSION

Nonequilibrium Crystallization of Augite

Our observations by analytical TEM showed significant compositional variation in the augite grains at a micrometer scale. The compositions fluctuate between Wo_{20} and Wo_{50} , even within a single grain. Fluctuations of composition in Ca-rich pyroxenes from porphyritic chondrules have been reported previously (Jones 1994, 1996). In type I chondrules, Jones (1994) measured in Ca-rich pyroxene a mean Ca content varying from Wo_{32} to Wo_{44} from one grain to another. This can be largely attributed to growth zoning, the evolution of liquid compositions leading to enrichment in Ca, as well as Fe and other less compatible trace elements, from core to rim of the augite crystals. The composition jumps at subgrain boundaries suggest that sector zoning occurred by steps with successive overgrowths and that the crystallization conditions were metastable with probable high undercooling.

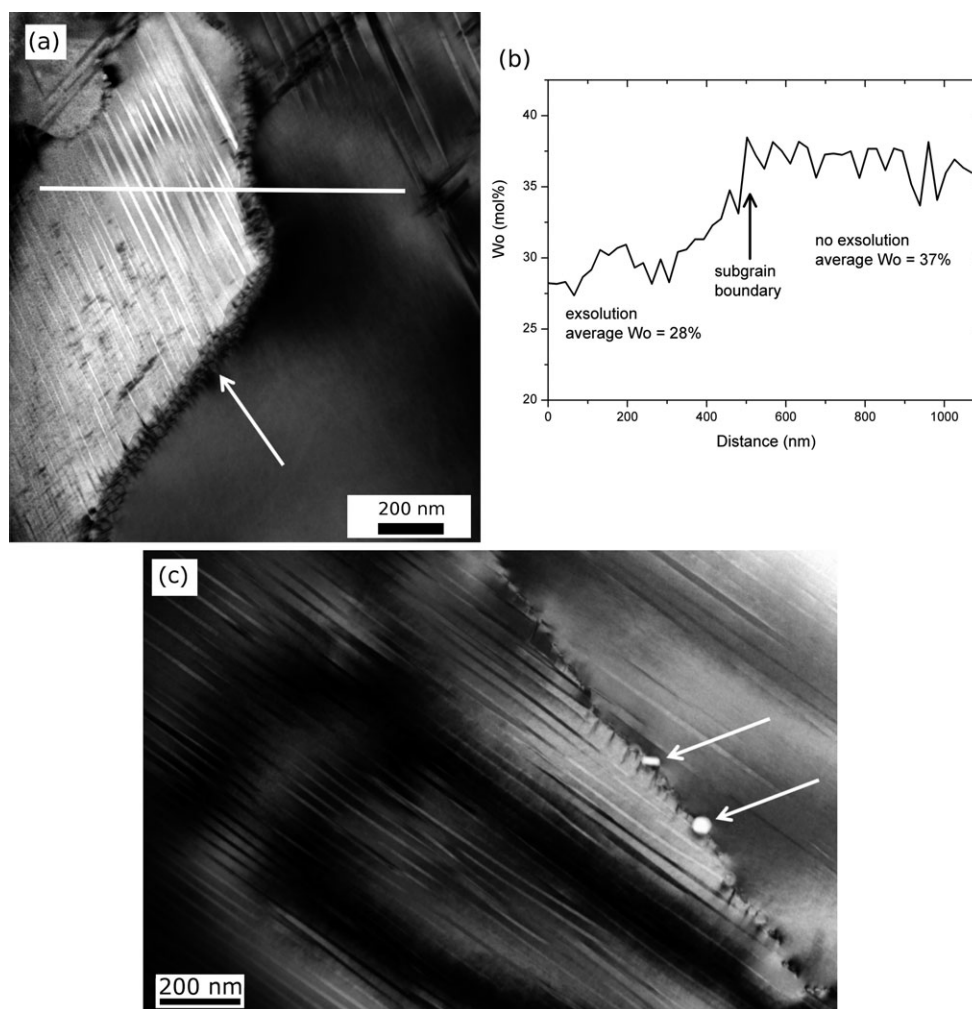


Fig. 5. Subgrain boundaries in pyroxene. a) Bright-field TEM image of a subgrain boundary (white arrow) in the P2 chondrule. This subgrain boundary delimits two areas with different microstructures. The left part contains exsolution lamellae, while the right part is free of them. b) Composition profile across the subgrain boundary, marked by a white line on the TEM image. Note the sharp composition step at the subgrain boundary, from an average composition Wo_{28} on the left side (with exsolution lamellae) to Wo_{37} at the right side (without exsolution lamellae). c) Bright-field TEM image of a subgrain boundary in the R2 chondrule. Note the presence of precipitates (white arrows) connected to the subgrain boundary. They show strong enrichment in SiO_2 .

Relation between Composition and Microstructure

Our study showed a strong correlation between the local composition and the microstructure (Fig. 4). The composition overlaps between the limits of the different microstructure domains are likely related to the growth metastability discussed above, due to undercooling during rapid cooling of chondrules. The presence of minor elements might also be a cause for blurring the limits of the miscibility gap (Lindsley 1983). The mean compositions of the exsolved zones are mostly between Wo_{20} and Wo_{35} . This composition range corresponds to the two-phase field augite + pigeonite just below the crystallization temperature (e.g., Carlson [1988] for the

$Mg_2Si_2O_6$ - $CaMgSi_2O_6$ phase diagram). The formation of exsolution started just after the crystallization of augite at a temperature close to 1350 °C or lower because of rapid cooling and undercooling. The formation mechanism of exsolution in pyroxene has been widely studied and many descriptions can be found in the literature (e.g., Buseck et al. 1980; Putnis 1992). Exsolution lamellae in Ca-pyroxene occur as crystallographically oriented intergrowths. The lamellae result from subsolidus re-equilibration during cooling when the Ca-pyroxene grains enter the two pyroxene phase field. The width and spacing of lamellae mainly depend on the cooling rate. The exsolution size distribution shown in Fig. 6 likely reflects compositional

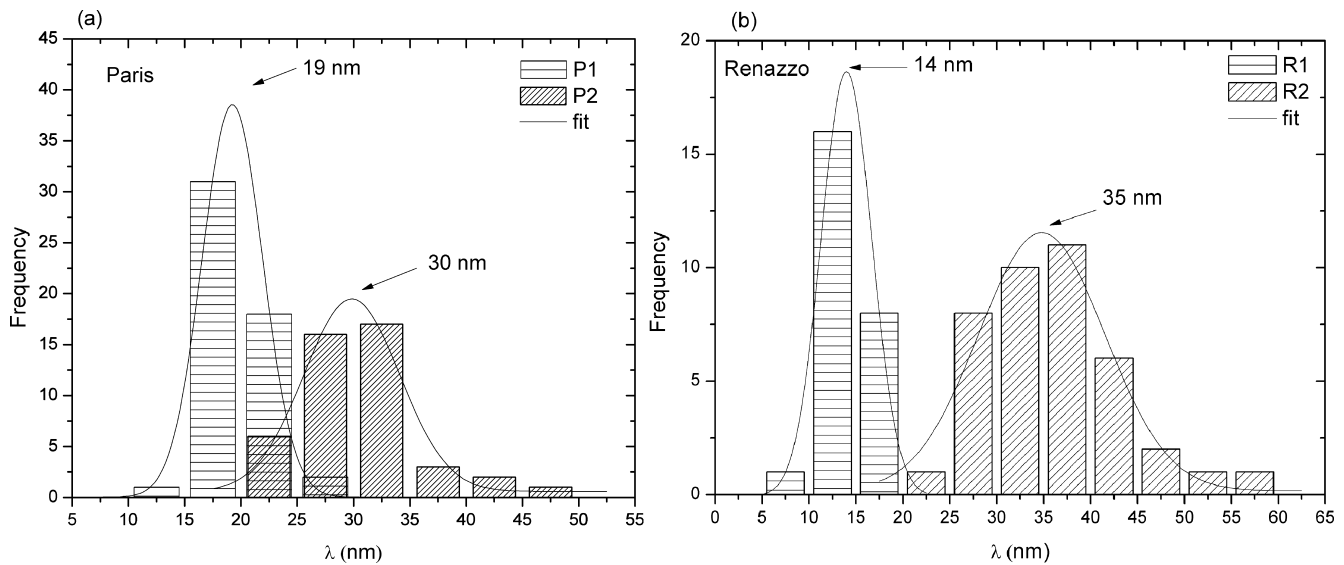


Fig. 6. Frequency diagrams showing the distribution of the lamella wavelength measured in (a) Paris and (b) Renazzo for areas of 500 nm^2 . The distributions of the lamella wavelength have a Gaussian shape centered on 19 nm for P1 and 30 nm for P2. In Renazzo, distributions are centered at 14 nm for R1 and 35 nm for R2.

Table 2. Summary of the exsolution lamella characteristics in each chondrule from the Paris and Renazzo chondrites. The standard deviation is calculated from the Gaussian fit of the lamellae wavelengths distribution shown in Fig. 7.

Chondrule	Lamella wavelength range (nm)	Gaussian peak lamella value (nm)	Standard deviation at 1σ (nm)
P1	10–30	19	3
P2	20–50	30	4
R1	5–20	14	3
R2	20–60	35	7

differences caused by local disequilibrium effects. However, the spread of exsolution sizes remains low and is not larger than what it is experimentally observed in annealed samples under isothermal conditions and comparable compositions (Weinbruch et al. 2006). For areas with higher Ca concentration, centered on Wo_{40} , the microstructure is dominated by a nanometer-scaled tweed texture. Areas with these compositions entered in the two-phase field pigeonite + augite at lower temperature than the well-developed exsolved areas, according to the $\text{Mg}_2\text{Si}_2\text{O}_6$ - $\text{CaMgSi}_2\text{O}_6$ phase diagram (e.g., Carlson 1988). The exsolution process, which is diffusion controlled, is thus significantly reduced in amplitude leading to a small wavelength-modulated texture. Finally, the highest Ca-rich compositions (above $\sim\text{Wo}_{40}$) do not exhibit any exsolution microstructure. Given the relatively high cooling rates

of chondrules, the corresponding augite grains or local areas within grains have never been able to develop exsolution microstructure because the solvus is crossed at too low temperature to allow further atomic diffusion of significant distances.

Determination of the Cooling Rates

Exsolution phenomena are diffusion controlled and thus are time and temperature dependent. Experimental calibrations provide information on the thermal history of the rock and in particular their cooling history from high-temperature domains between $1350 \text{ }^\circ\text{C}$ and $1000 \text{ }^\circ\text{C}$. In particular, the spacing and thickness of exsolution lamellae can be used to estimate the cooling rate (e.g., McCallister 1978; Grove 1982; Fukada et al. 1987; Weinbruch and Müller 1995; McCallum and O'Brien 1996; Weinbruch et al. 2001; Leroux et al. 2004, 2008).

Based on an experimental work of McCallister (1978), Weinbruch and Müller (1995) calculated the time–temperature–transformation (TTT) diagram associated with the growth of exsolution lamellae in dynamic systems (i.e., coarsening rates depending on the temperature). From this TTT diagram, they deduced calibration curves for estimated cooling rates, assuming an initial temperature of $1350 \text{ }^\circ\text{C}$. For complex multicomponent chondrule melt, the appearance of Ca-pyroxene likely occurred at lower temperature (e.g., Wick and Jones 2012). As noted by Weinbruch and Müller (1995), the estimation of cooling rates strongly

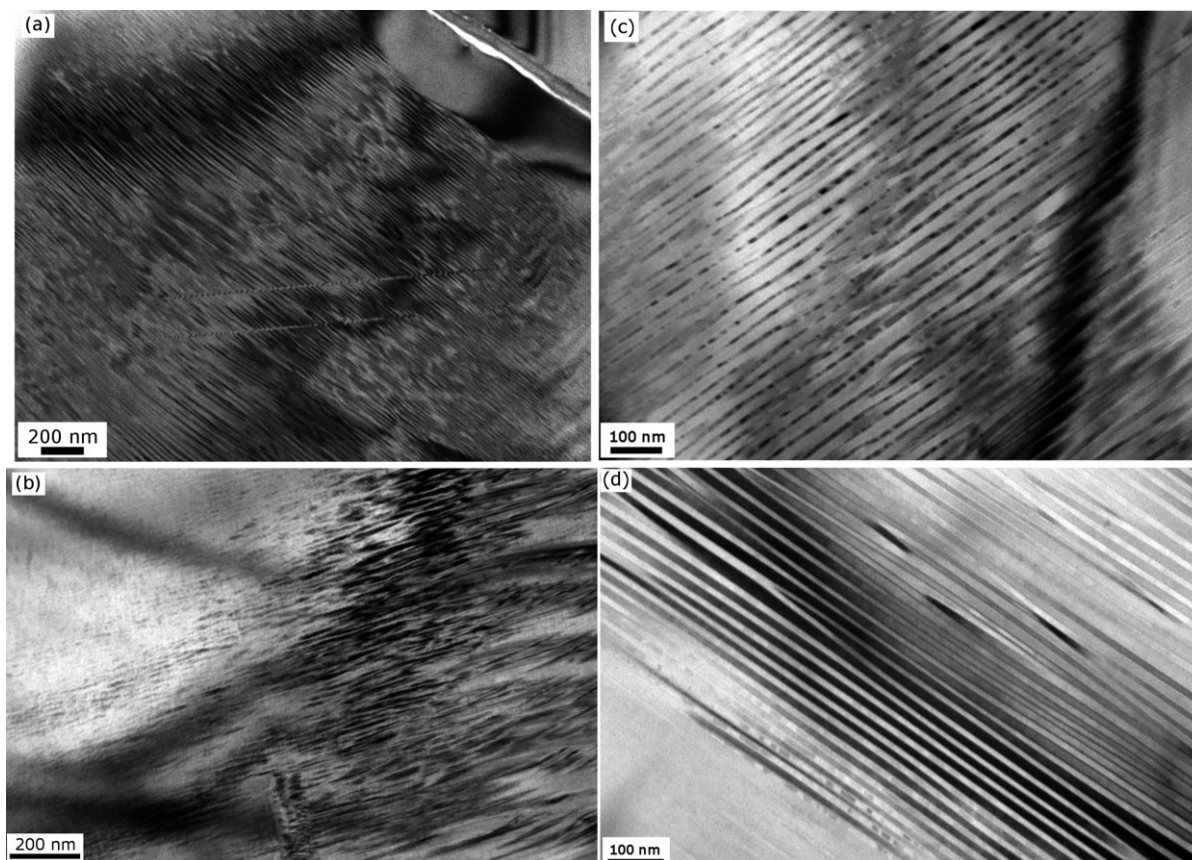


Fig. 7. Bright-field TEM images of exsolution lamellae on (001). a) Fine exsolution lamellae in chondrule P1, average wavelength 19 nm. b) Fine exsolution lamellae in chondrule R1, average wavelength 14 nm. c) Well-developed exsolution lamellae in chondrule P2, average wavelength 30 nm. d) Exsolution lamellae in chondrule R2, average wavelength 35 nm.

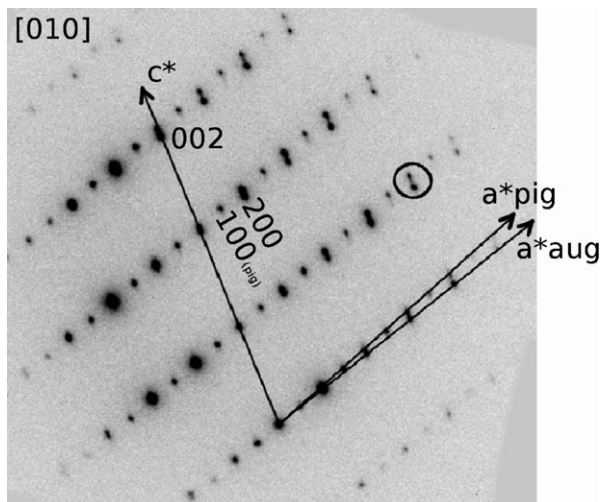


Fig. 8. SAED pattern including pigeonite lamellae and the augite host (in P2). The pattern exhibits $h+k$ odd spots corresponding to the pigeonite $P2_1/c$ and splitting of spots due to the variation of the β angle between the monoclinic augite $C2/c$ and the monoclinic pigeonite $P2_1/c$.

depends on the initial temperature at which the exsolutions start to form; the lower the temperature, the lower the cooling rate for a given exsolution microstructure. Finally, it should also be noted that this diagram is applicable to “thin” lamella wavelength (\approx below 40 nm) and allows an estimation of cooling rates between 1350 °C and 1200 °C (below this temperature, the diffusion becomes too slow to account for coarsening).

At first glance, the measured spacing between lamellae seems relatively widely spread (Table 2). However, the distribution is not homogeneous and most of the lamella wavelengths are centered on average values (Fig. 6). A comparable dispersion was measured by Weinbruch et al. (2006) for isothermal annealing of synthetic Fe-free clinopyroxene of composition $En_{45}Di_{55}$. The distributions roughly have a Gaussian shape. For the associated uncertainties, we considered the wavelength value at the Gaussian peak plus or minus the standard deviation at 1σ . The wavelength ranges for each chondrule are 19 ± 3 nm for P1,

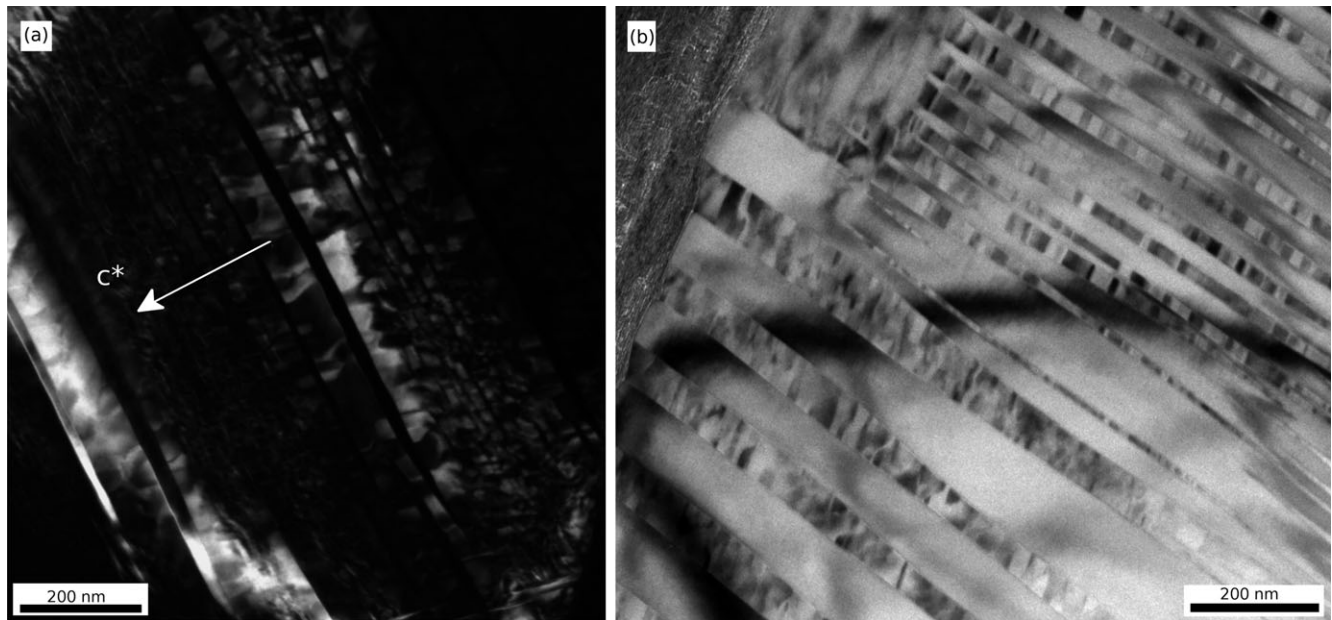


Fig. 9. Antiphase boundaries (APBs) in pigeonite lamellae. a) Dark-field image from P2 in a pigeonite area containing augite lamellae. Augite lamellae appear in black (image recorded with an $h+k$ odd reflection) and pigeonite lamellae exhibit a variable contrast due to the APBs. b) Bright-field image of APBs in R2 present in the pigeonite lamellae within the augite host. APBs are preferentially oriented along (100). Note that the bottom-left side on the image contains exsolution lamellae that are anomalously thick, while in the upper right side, the lamellae have a spacing close to the average of this sample (35 nm).

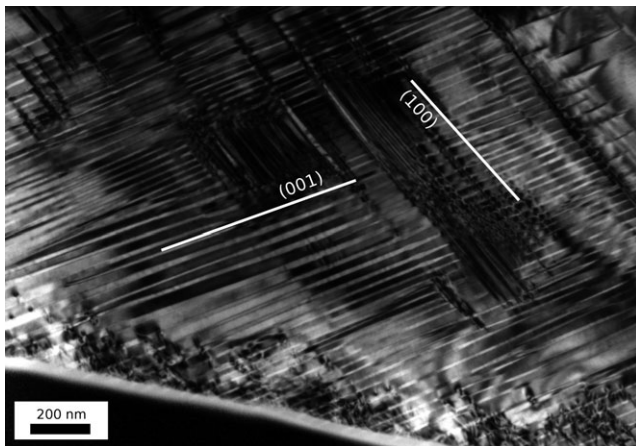


Fig. 10. Bright-field TEM image showing an area in chondrule P2 with exsolution lamellae on (001) and (100). Note that the lamellae in (100) are heterogeneously distributed, while those on (001) have a regular spacing.

30 ± 4 nm for P2, 14 ± 3 nm for R1, and 35 ± 7 nm for R2 (see column 2 in Table 2). To estimate cooling rates associated with the measured wavelengths, we have used the modeling of the growth of exsolution lamellae done by Weinbruch and Müller (1995). For different cooling rates, Fig. 12 shows the value of wavelengths of lamellae as a function of temperature. We deduced cooling rates in Paris within the range of

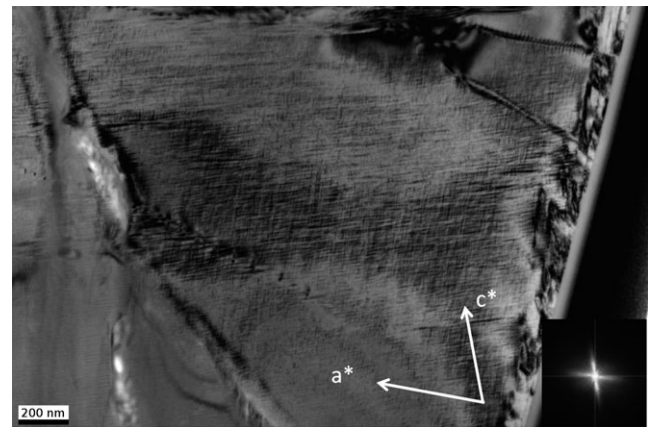


Fig. 11. Bright-field image of the “tweed” microstructure in P1. The Fourier transform of this area, inserted at the bottom-right side of the picture, shows the two directions a^* and c^* .

$60\text{--}580$ °C h^{-1} for P1, $7\text{--}25$ °C h^{-1} for P2, 370 °C to thousands of °C h^{-1} for R1, and $3\text{--}17$ °C h^{-1} for R2. These cooling rates are within the same range as those of type II chondrules, i.e., $1\text{--}1000$ °C h^{-1} , inferred from petrologic experiments (e.g., Hewins et al. 2005; Wick and Jones 2012), as well as those of type I chondrules, i.e., $0.1\text{--}400$ °C h^{-1} , recently calculated using Cu-Ga zoning profiles in metal grains (Humayun 2012). This

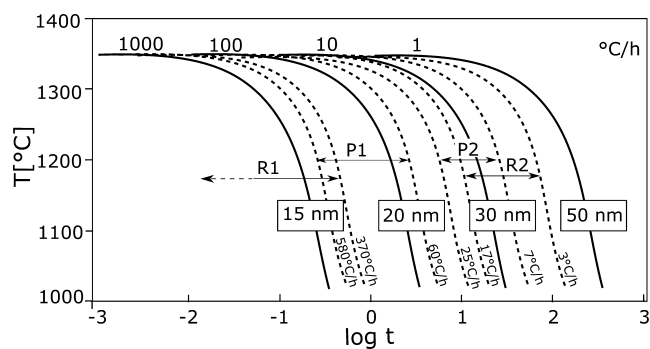


Fig. 12. Diagram showing the cooling rate curves, adapted from fig. 4 of Weinbruch and Müller (1995). The solid curves correspond to cooling rates of 1000, 100, 10, and 1 °C h⁻¹ for a pyroxene with a composition of Wo₂₇, and attached numbers in boxes give the corresponding lamella wavelengths at 1200 °C. The measured lamella wavelengths in Paris are mainly between 16 and 22 nm for P1 and between 26 and 34 nm for P2 corresponding to cooling rates within the range of 60–580 °C h⁻¹ and 7–25 °C h⁻¹, respectively (dashed lines). For Renazzo, the measured lamella wavelengths are mostly between 11 and 17 nm for R1 and 28 and 42 nm for R2 corresponding to cooling rates within the range of 370 °C h⁻¹ to thousands °C h⁻¹ and 3–17 °C h⁻¹, respectively (dashed lines). For all deduced cooling rate values, an initial temperature of 1350 °C, a linear cooling, and a closure temperature of 1200 °C were assumed. The temperature offset between the Paris and Renazzo chondrule values is for clarity.

may indicate that the formation of type I and type II chondrules in the proto-solar nebula had a common mechanism.

CONCLUSION

We have studied exsolution features at the nanometer scale in Ca-rich pyroxenes within type IAB porphyritic chondrules from the Paris and Renazzo carbonaceous chondrites in order to constrain cooling rates of type I chondrules. Our analytical TEM study reveals that the microstructure of the augite grains is highly variable and strongly depends on the local composition of the grains. These compositional variations are likely due to nonequilibrium crystallization of augite. The local composition is closely related to three different microstructures, including (1) un-exsolved grains which have a Wo content higher than Wo₄₀ or lower than Wo₁₀, (2) exsolved grains whose Wo content is typically between Wo₃₃ and Wo₂₀, and (3) tweed textured grains with an intermediate Wo content close to Wo_{35–45} and Wo₁₀.

The exsolution lamella wavelengths measured in augite grains exhibit a Gaussian frequency distribution within all of the chondrules studied. We determined a characteristic value for the lamella wavelength for each chondrule and we deduced the cooling rates of type I chondrules from the Paris (chondrules P1 and P2) and

Renazzo (chondrules R1 and R2) chondrites. The characteristic values are 19 ± 3 nm for P1, 30 ± 4 nm for P2, 14 ± 3 nm for R1, and 35 ± 7 nm for R2. Based on modeling of exsolution growth by Weinbruch and Müller (1995), these values correspond to cooling rates of 60–580 °C h⁻¹ and 7–25 °C h⁻¹ for Paris (P1 and P2, respectively) and from 370 °C to thousands of °C h⁻¹ and 3–17 °C h⁻¹ for Renazzo (R1 and R2, respectively). These ranges are compatible with type II chondrule cooling rates (~1–1000 °C h⁻¹) and those of previous studies of type I chondrules, and favor the hypothesis of a common mechanism of formation in the protosolar nebula occurring in different oxidizing environments.

Acknowledgments—The authors thank the MNHN for the samples. The authors also thank J. F. Dhenin and A. Addad for their assistance at the Lille (France) electron microscopy facility. They thank D. Troadec for the preparation of high-quality FIB sections. The TEM work has been done at the electron microscope facility at Lille University with the support of Chevreul Institute, the European FEDER, and the Région Nord-Pas-de-Calais (France). This work was supported by the French ANR Program THEODULE (ANR-12-BS05-0010). We thank R. Jones, an anonymous reviewer, and the associate editor A. Ruzicka for very constructive comments that deeply improved the clarity of the manuscript.

Editorial Handling—Prof. Alexander Ruzicka

REFERENCES

- Buseck P. R., Nord G. L. Jr., and Veblen D. R. 1980. Subsolidus phenomena in pyroxenes. In *Pyroxenes*, edited by Prewitt C. T. Reviews in Mineralogy, vol. 7. Washington D.C.: Mineralogical Society of America. pp. 117–211.
- Carlson W. D. 1988. Subsolidus phase equilibria on the forsterite-saturated join Mg₂Si₂O₆-CaMgSi₂O₆ at atmospheric pressure. *American Mineralogist* 73:232–241.
- Carpenter M. A. 1979. Contrasting properties and behaviour of antiphase domains in pyroxenes. *Physics and Chemistry of Minerals* 5:119–131.
- Chaumard N., Humayun M., Zanda B., and Hewins R. H. 2014. Cooling rate of a type I chondrule from the Renazzo CR2 chondrite inferred from Cu and Ga diffusion profiles in metal grains (abstract #2448). 45th Lunar and Planetary Science Conference. CD-ROM.
- Chaumard N., Humayun M., Zanda B., and Hewins R. H. 2015. Cooling rates of type I chondrules from the Renazzo CR2 chondrite: Implications for chondrule formation (abstract #1907). 46th Lunar and Planetary Science Conference. CD-ROM.
- Fukada K., Yamanaka T., and Takonami N. 1987. Dependence of exsolution textures in synthetic augite on

- its composition and cooling rate. *Mineralogical Journal* 13:376–389.
- Grove T. L. 1982. Use of exsolution lamellae in lunar clinopyroxenes as cooling rate speedometers: An experimental calibration. *American Mineralogist* 67:251–268.
- Hewins R. H., Jones R. H., and Scott E. R. D. 1996. *Chondrules and the protoplanetary disk*. Cambridge, UK: Cambridge University Press. ISBN 0-521-55288-5.
- Hewins R. H., Connolly H. C. Jr., Lofgren G. E., and Libourel G. 2005. Experimental constraints on chondrule formation. In *Chondrites and the protoplanetary disk*, edited by Krot A. N., Scott E. R. D., and Reipurth B. San Francisco, California: ASP Conference Series. pp. 286–316.
- Hewins R. H., Bourrot-Denise M., Zanda B., Leroux H., Barrat J.-A., Humayun M., Göpel C., Greenwood R. C., Franchi I. A., Pont S., Lorand J.-P., Cournède C., Gattacceca J., Rochette P., Kuga M., Marrocchi Y., and Marty B. 2014. The Paris meteorite, the least altered CM chondrite so far. *Geochimica et Cosmochimica Acta* 124:190–222.
- Humayun M. 2012. Chondrule cooling rates inferred from diffusive profiles in metal lumps from the Acfer 097 CR2 chondrite. *Meteoritics & Planetary Science* 47:1191–1208.
- Jones R. H. 1990. Petrology and mineralogy of type II, FeO-rich chondrules in Semarkona (LL3.0): Origin by closed-system fractional crystallization, with evidence for supercooling. *Geochimica et Cosmochimica Acta* 54:1785–1802.
- Jones R. H. 1994. Petrology of FeO-poor, porphyritic pyroxene chondrules in the Semarkona chondrite. *Geochimica et Cosmochimica Acta* 58:5325–5340.
- Jones R. H. 1996. FeO-rich, porphyritic pyroxene chondrules in unequilibrated ordinary chondrites. *Geochimica et Cosmochimica Acta* 60:3115–3138.
- Jones R. H. and Lofgren G. E. 1993. A comparison of FeO-rich, porphyritic olivine chondrules in unequilibrated chondrites and experimental analogues. *Meteoritics* 28:213–221.
- Jones R. H. 1996. FeO-rich, porphyritic pyroxene chondrules in unequilibrated ordinary chondrites. *Geochimica et Cosmochimica Acta* 60:3115–3138.
- Leroux H., Devouard B., Cordier P., and Guyot F. 2004. Pyroxene microstructure in the Northwest Africa 856 Martian meteorite. *Meteoritics & Planetary Science* 39:711–722.
- Leroux H., Jacob D., Stodolna J., Nakamura-Messenger K., and Zolensky M. E. 2008. Igneous Ca-rich pyroxene in comet 81P/Wild 2. *American Mineralogist* 93:1933–1936.
- Lindsley D. H. 1983. Pyroxene thermometry. *American Mineralogist* 68:477–493.
- Lofgren G. E. 1996. A dynamic crystallization model for chondrule melts. In *Chondrules and the protoplanetary disk*, edited by Hewins R. H., Jones R. H., and Scott E. R. D. Cambridge, UK: Cambridge University Press. pp. 187–196.
- McCallister R. 1978. The coarsening kinetic associated with exsolution in an iron-free clinopyroxene. *Contributions to Mineralogy and Petrology* 65:327–331.
- McCallum I. S. and O'Brien H. E. 1996. Stratigraphy of the lunar highland crust: Depths of burial of lunar samples from cooling-rate studies. *American Mineralogist* 81:1166–1175.
- Miyamoto M., Mikouchi T., and Jones R. H. 2009. Cooling rates of porphyritic olivine chondrules in the Semarkona (LL3.00) ordinary chondrite: A model for diffusional equilibration of olivine during fractional crystallization. *Meteoritics & Planetary Science* 44:521–530.
- Morimoto N. and Tokonami M. 1969. Domain structure of pigeonite and clinoenstatite. *American Mineralogist* 54:1101–1117.
- Putnis A. 1992. *Introduction to mineral sciences*. Cambridge, UK: Cambridge University Press. 457 p.
- Radomsky P. M. and Hewins R. H. 1990. Formation conditions of pyroxene-olivine and magnesian olivine chondrules. *Geochimica et Cosmochimica Acta* 54:3475–3490.
- Tribaudino M. 2000. A transmission electron microscope investigation of the $C2/c \rightarrow P2_1/c$ phase transition in clinopyroxenes along the diopside-enstatite ($\text{CaMgSi}_2\text{O}_6\text{-Mg}_2\text{Si}_2\text{O}_6$) join. *American Mineralogist* 85:707–715.
- Van Cappellen E. 1990. The parameterless correction method in X-ray microanalysis. *Microscopy Microanalysis Microstructures* 1:1–22.
- Van Cappellen E. and Doukhan J.-C. 1994. Quantitative transmission X-ray microanalysis of ionic compounds. *Ultramicroscopy* 53:343–349.
- Watanabe S., Kitamura M., and Morimoto N. 1985. A transmission electron microscope study of pyroxene chondrules in equilibrated L-group chondrites. *Earth and Planetary Science Letters* 72:87–98.
- Weinbruch S. and Müller W. F. 1995. Constraints on the cooling rates of chondrules from the microstructure of clinopyroxene and plagioclase. *Geochimica et Cosmochimica Acta* 59:3221–3230.
- Weinbruch S., Müller W. F., and Hewins R. H. 2001. A transmission electron microscope study of exsolution and coarsening in iron-bearing clinopyroxene from synthetic analogues of chondrules. *Meteoritics & Planetary Science* 36:1237–1248.
- Weinbruch S., Styrsky V., and Dirsch T. 2006. The size distribution of exsolution lamellae in iron-free clinopyroxene. *American Mineralogist* 91:551–559.
- Weisberg M. K., Prinz M., Clayton R. N., and Mayeda T. K. 1993. The CR (Renazzo-type) carbonaceous chondrite group and its implications. *Geochimica et Cosmochimica Acta* 57:1567–1586.
- Wick M. J. and Jones R. H. 2012. Formation conditions of plagioclase-bearing type I chondrules in CO chondrites: A study of natural samples and experimental analogs. *Geochimica et Cosmochimica Acta* 98:140–159.
- Zanda B. 2004. Chondrules. *Earth and Planetary Science Letters* 224:1–17.